On the issue of the PEMFC operating fault identification: Generic analysis tool based on voltage pointwise singularity strengths

Djedjiga Benouioua, Denis Candusso, Fabien Harel, Pierre Picard, Xavier Francois

Work presented at ICEREGA 2017 – Belfort, France
Journal selection, ID254
Managing Guest Editor of IJHE: Dr. Mohamed BECHERIF

On the issue of the PEMFC operating fault identification: generic analysis tool based on voltage pointwise singularity strengths

D. Benouioua[1, 2, 3, 4*], **D. Candusso**[1, 2, 3], **F. Harel**[3, 5], **P. Picard**[6], **X. François**[7]
[1] ITE EFFICACITY, 14-20 boulevard Newton, Champs-sur-Marne, 77447 Marne la Vallée, France.
[2] IFSTTAR / COSYS / SATIE, UMR CNRS 8029, 25 allée des marronniers, 78000 Versailles Satory, France.
[3] FCLAB, FR CNRS 3539, rue Ernest Thierry Mieg, 90010 Belfort Cedex, France.
[4] FEMTO-ST, UMR CNRS 6174, University of Bourgogne Franche-Comté, 25030 Besançon Cedex, France.
[5] University of Lyon, IFSTTAR / AME / LTE, 25 avenue François Mitterrand, Case24, 69675 Bron Cedex, France.
[6] ENGIE - CRIGEN, 361 avenue du Président Wilson BP 33, 93211 La Plaine Saint-Denis, France.
[7] University of Technology Belfort – Montbéliard (UTBM), rue Ernest Thierry Mieg, 90010 Belfort Cedex, France.

* Corresponding author:
djedjiga.benouioua@femto-st.fr

Tel: 0033 3 84 58 36 33
Fax: 0033 3 84 58 36 36

Other email addresses:
denis.candusso@ifsttar.fr
fabien.harel@ifsttar.fr
pierre-2.picard@engie.com
xavier.francois@utbm.fr

Abstract:
The purpose of this article is to study the portability of a non-intrusive and free of any external / internal disturbance diagnosis tool devoted to the monitoring of the State of Health (SoH) of PEM Fuel Cell (PEMFC) stack. The tool is based on a thorough analysis of the stack voltage signal using a multifractal formalism and wavelet leaders. It offers well-suited signatures indicators on the SoH of the Fuel Cell. Some relevant descriptors extracted from these patterns (singularity features) are used in the frame of Machine Learning approaches to allow the PEMFC fault identification. The proposed diagnosis strategy is evaluated with two different PEMFC stacks. The first one is designed for automotive applications and the second one is dedicated to stationary use (micro combined heat and power - µCHP application). The classification results obtained for the both stacks indicate that the proposed PEMFC diagnosis tool allows identifying simple operating faults as well as more complicated operating situations combining several fault types.

Keywords:
PEMFC stacks; automotive application; µCHP application; Diagnostic; Voltage Singularity Spectrum; Machine Learning.

1. Introduction

Fuel cells (FC) are considered as a promising alternative way for energy conversion [1]. To ensure their durability, reliability and safety, many fault diagnosis and fault tolerant control methods have been proposed. These methods can be classified into two groups: model-based methods [2-5] and data-driven methods [6-8]. The methods of the first group are very cumbersome and complex because they require an in-depth knowledge of the multi-physical mechanisms (thermal, electrical, electrochemical, and fluidic ones) which can occur in FC systems. They are based on numerous parameters governing its operation, and their values are difficult to estimate. Some model-based methods allows a deeper understanding of the FC physics but they might be not suitable to provide an accurate / quantitative description of the FC performances. Hence, the data-driven techniques attract more and more attention because of their simplicity regarding the implementation and the good performances obtained without profound system structure knowledge. They are supported by efficient signal processing methods as: Fourier transform [9], multi-resolution analysis [10, 11], singularity analysis [12, 13]. For fault identification and isolation tasks, some works use Electrochemical Impedance Spectra (EIS) as normal or faulty operation signatures to supply artificial intelligence algorithms (based for instance on fuzzy logic [14] or neural networks [15]) or conventional pattern recognition approaches (based on Support Vector Machines (SVM) [16], K-Nearest Neighbors (KNN) [13] methods).
This work aims at studying the portability of an innovative data driven approach dedicated to PEMFC diagnosis, named singularity analysis. This method consists in analyzing the pointwise singularities stamped in the stack voltage signal for various FC operating conditions. The singularity features are then summarized in the form of concave arcs estimated thanks to a set of mathematical equations, baptized multifractal formalism [17-19]. The advanced analysis tool, named Voltage Singularity Spectrum (VSS) is then obtained using a non-intrusive manner and without affecting in any way the FC operation. Indeed, no external additional AC-solicitation has to be superimposed to the existing DC load current as it is the case in the usual EIS operation mode.
This paper is organized as follow. Section 2 deals with the experimental work and environment conducted with two PEMFC stacks. In section 3, a brief mathematical foundation of the singularity measurement is given. In section 4, we show how it is possible to make the singularity spectrum combined with Machine Learning techniques as a PEMFC diagnosis tool. Then, the portability of the proposed tool is discussed. Main conclusions are given in Section 5.

2. Experimental

2.1. Synopsis of the investigated PEM Fuel Cells

In our study, two PEMFC stacks are experimented to evaluate the portability of the proposed diagnosis tool. The first one is an 8 cell stack designed for automotive applications and manufactured by CEA (Alternative Energies and Atomic Energy Commission). The second one is a 12 cell stack dedicated to stationary application (micro Combined Heat and Power - µCHP

application). It is designed and marketed by Riesaer Brennstoffzellentechnik GmbH and Inhouse Engineering GmbH, Germany.
The first stack ($PEMFC_{Auto}$) is made of metallic gas distributor plates. The electrode active surface of a cell is equal to 220 cm^2. It is fed by air at cathode and pure hydrogen (H_2) at anode. A summary of the FC nominal operating conditions is given in Table 1. The stack operates with a nominal current of 110 A. A picture of the stack is shown in Fig. 1(a).
The second stack ($PEMFC_{\mu CHP}$) is fed by air at cathode, and at anode by a fuel mixture (75 % of H_2 and 25 % of carbone dioxide - CO_2) simulating a reformat. It is made of graphite gas distributor plates. The active surface of the electrode is 196 cm^2. The stack operates with a nominal current of 80 A. A picture of the stack is given in Fig. 1(b). A summary of the FC nominal operating parameters and other main characteristics are given in Table 2.

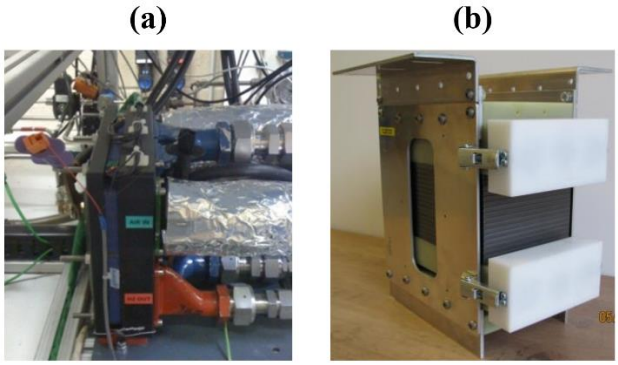

Fig. 1. Pictures of the two investigated PEMFC stacks:
a) 8 cell stack designed for automotives ($PEMFC_{Auto}$),
b) 12 cell stack designed for µCHP operation ($PEMFC_{\mu CHP}$).

Table 1. $PEMFC_{Auto}$ nominal operating conditions.

Coolant flow: deionized water	2 l/min
Anode stoichiometry rate (H_2)	1.5
Cathode stoichiometry rate (air)	2
Absolute pressure for H_2 and air inlets	150 kPa
Max. anode - cathode pressure gap	30 kPa
Temperature of the cooling circuit	80°C
Anode and cathode relative humidity rate	50 %
Nominal Current	110 A

Table 2. $PEMFC_{\mu CHP}$ nominal operating conditions.

Coolant flow: deionized water	3 l/min
Anode stoichiometry rate (H_2 and CO_2 mix)	1.3
Cathode stoichiometry rate (air)	2
Absolute pressure for H_2 and air inlets	150 kPa
Max. anode - cathode pressure gap	20 kPa
Temperature of the cooling circuit	75°C
Anode and cathode relative humidity rate	50 %
Nominal Current	80 A

2.2. Experimental process

The above described PEMFCs were experimented with testbenches developed in the FC platform of Belfort, France. It includes mainly:

- a complete gas conditioning sub-system with gas humidifiers at anode and cathode,
- a test stand section dedicated to the control of the temperature inside the stack and including the FC primary water circuit,
- an electric / electronic management sub-system,
- an electronic load.

The monitoring and the control of the FC testbenches parameters are done through National Instruments materials and a dedicated software. A Human-Machine Interface (HMI) was also developed in-lab using Labview^{TM}.

The purpose of the experimental protocol was to introduce different controlled health states into the PEMFC stacks by configuring various operating parameters. Two PEMFC health states were set: no stack failure state (when the FC is operating under normal parameters - Ref) and with stack failure state (when the FC is operating under abnormal / severe parameters).

Different scenarios of FC system failure were associated to the changing of different setting physical parameters through the control-command interface of the testbenches, namely: cathode stoichiometry rate (FSC), anode stoichiometry rate (FSA), gas pressure at anode and cathode (P), cooling circuit temperature (T), and relative humidity level (RH) at anode and cathode (by controlling the gas dew point temperatures).

The fault scenarios considered in this work were selected in the framework of two projects: the DIAPASON2 project supported by the French National Research Agency (ANR) and the "Decentralized energy production" project directed by EFFICACITY, the French R&D Institute for urban energy transition. The fault scenarios duplicate various failures that are representative of the application environment (electric vehicle or stationary generator). The faults considered correspond mainly to potential ineffective operations of the FC system ancillaries / actuators or sensors used in the Balance-of-Plant (e.g. failure of the air supply subsystem in the FC generator related with the FSC parameter). The parameter levels of the faulty modes were specified with the help of the PEMFC manufacturers (CEA LITEN in Grenoble - France for the $PEMFC_{Auto}$ stack, and RBZ / Inhouse Engineering GmbH in Berlin - Germany for the $PEMFC_{\mu CHP}$ stack). The trade-offs concerning the parameter ranges explored, the selected parameter levels have been found by considering the capabilities of the FC in terms of performance (a total FC collapse or severe FC stack degradations had to be avoided), by taking into account the technological limitations of the FC test stands, and the possible duration of the experimental campaigns as well.

The set of the tests performed, with the two stacks and according to the degrading operating parameters, is reported in Table 3.

Table 3. The set of FC operating conditions applied during the experimentation of the two stacks: **Ref**: normal conditions - **DFSC**: cathode flow fault - **DFSA**: anode flow fault - **DP**: gas pressure fault - **DT**: cooling circuit temperature fault - **DRH**: gas dew point temperature fault - **DCO**: carbon monoxide poisoning (H_2+CO).
The underlined parameter values correspond to the introduced faults.
The notation 'ND' means that the experiment is Not Done.

	Ref		DFSC		DFSA		DP		DT		DRH		DCO	
	Auto	µCHP	Auto	µCHP	Auto	µCHP	Auto	µCHP	Auto	µCHP	Auto	µCHP	Auto	µCHP
FSC	2	2	1.3	2.6 1.6	2	2	2	2	2	2	2	2	2	2
FSA	1.5	1.3	1.5	1.3	1.3	1.5 1.2	1.5	1.3	1.5	1.3	1.5	1.3	1.5	1.3
P (bar abs)	1.5	0.1	1.5	0.1	1.5	0.1	1.3	ND	1.5	0.1	1.5	0.1	1.5	0.1
T (°C)	80	70	80	70	80	70	80	70	75	72 65	80	70	80	70
RH (%)	50	50	50	50	50	50	50	50	50	50	ND	46 54	50	50
CO (ppm)	0	0	0	0	0	0	0	0	0	0	0	0	10	ND

3. Singularity measurement

Multifractals are the distribution of singularities, all lying on interwoven sets of varying fractal dimensions [20]. Multifractals arise in a variety of physical signals in the forms of self-similar sub-sets of samples, such as Multifractional Brownian Motion (MBM) signal [21], signals in turbulence [22], and temporal series in finance [23].
The singularity analysis, also named "multifractal analysis" allows the characterization of data by describing globally and geometrically the fluctuations of local regularity, usually measured by means of the Hölder exponent h.
It describes the time (t) based fluctuations of the signal given by a function $X(t)$. This is achieved by comparing the local variations of $X(t)$ around fixed time position t_0, against a local power law behavior: $X(t_0)$ is said to belong to $C^{\alpha}(t_0)$ with $\alpha \geq 0$ if there are a positive constant C and a polynomial P, satisfying $\deg(P) < \alpha$, such that $\left|X(t) - P_{t_0}(t)\right| \leq C|t - t_0|^{\alpha}$.
The Hölder exponent is defined as the largest α such as: $h(t_0) = \sup\{\alpha: X \in C^{\alpha}(t_0)\}$.
In practice, when $h(t_0)$ takes a value which tends to zero, the signal exhibits a strong singularity at t_0 (Fig. 2).

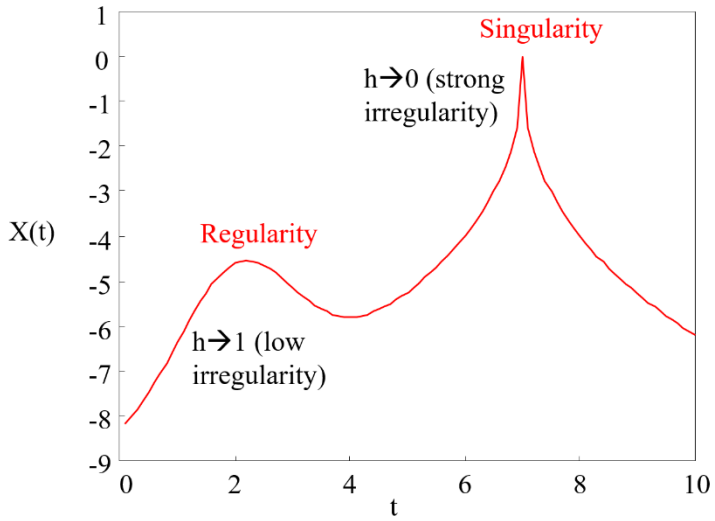

Fig. 2. Illustration of two pointwise regularity measures in the signal $X(t)$ quantified by the Hölder exponent h.

The singularity strength regarding the variability of the regularity of $X(t)$ vs. t is usually described through the so-called singularity spectrum. Building a singularity spectrum consists in associating to each Hölder exponent h the Hausdorff dimension $D(h)$ of the sets of points which exhibit the same value of h: $h \longmapsto D(h)$.
An example of singularity spectrum is given in Fig. 3.

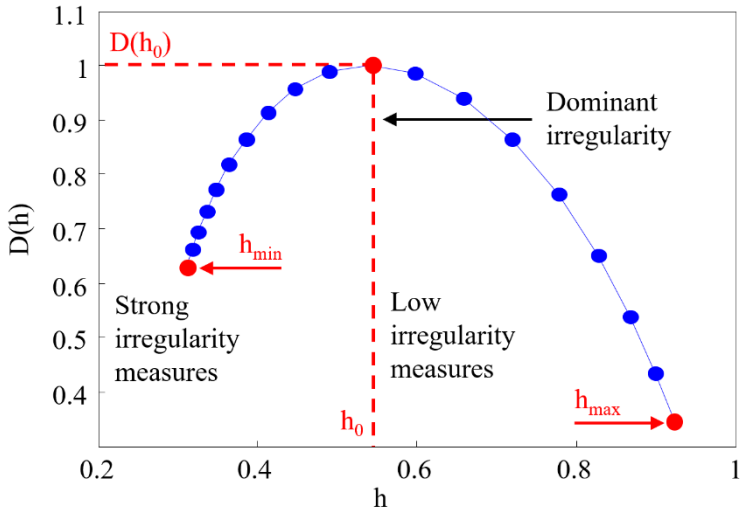

Fig. 3. Example of a singularity spectrum $D(h)$.

The numerical implementation of the mathematical formula can be achieved using the Wavelet Leaders Multifractal Formalism (WLMF).
Recently, a new formalism called wavelet leaders was proposed from the discrete wavelet transform [13,17-19]. Its mathematical basis can be described as follow.

Let us consider a function $\psi(t)$ with a compact time (t) support, called mother-wavelet, which satisfies the condition:

$\int_R t^i \psi(t)dt \neq 0$, where $i = 0, 1, \ldots, N_\psi - 1$ and the vanishing moment $N_\psi \geq 1$.

So, a family of wavelets $\psi^i(t)$ can be generated; it is sometimes called "daughter-wavelets". The templates of $\psi(t)$ dilated to scales 2^j and translated to time positions $2^j k$ where j is the multiresolution parameter, with an orthonormal basis of $L^2(R)$, can be formulated as follow [17-19]:

$$\psi_{j,k}(t) = \frac{1}{2^j}\psi\left(\frac{t-2^j k}{2^j}\right), j \in \mathbb{Z} \text{ and } k \in \mathbb{Z} \quad (1)$$

Then, the discrete wavelet transform of a signal $X(t)$ is defined by the following formula:

$$d_X(j,k) = \int_R X(t)2^{-j}\psi\left(2^{-j}t - k\right)dt \quad (2)$$

Assuming the dyadic interval λ and the dyadic cube Γ [17]:

$$\lambda = \left[k.2^j, (k+1).2^j\right] \quad (3)$$
$$\Gamma = 3\lambda = \lambda_{j,k-1} \cup \lambda_{j,k} \cup \lambda_{j,k+1} \quad (4)$$

Γ denotes the union of the interval λ with its two adjacent dyadic intervals [17]. Therefore, the wavelet leader is the local supremum of the wavelet coefficients located in the dyadic cube over all finer scales:

$$L_X(j,k) = \sup_{\lambda' \subset \Gamma}\left|d_{X,\lambda'}\right| \quad (5)$$

This equation indicates that to compute $L_X(j,k)$, which consists of the largest wavelet coefficient $d_X(j',k')$, we consider the indexes $(k-1)2^j \leq 2^{j'}k' < (k+2)2^j$ at all finer scales $2^{j'} \leq 2^j$. A possible scheme illustrating this definition is given in Fig. 4 [13,19].

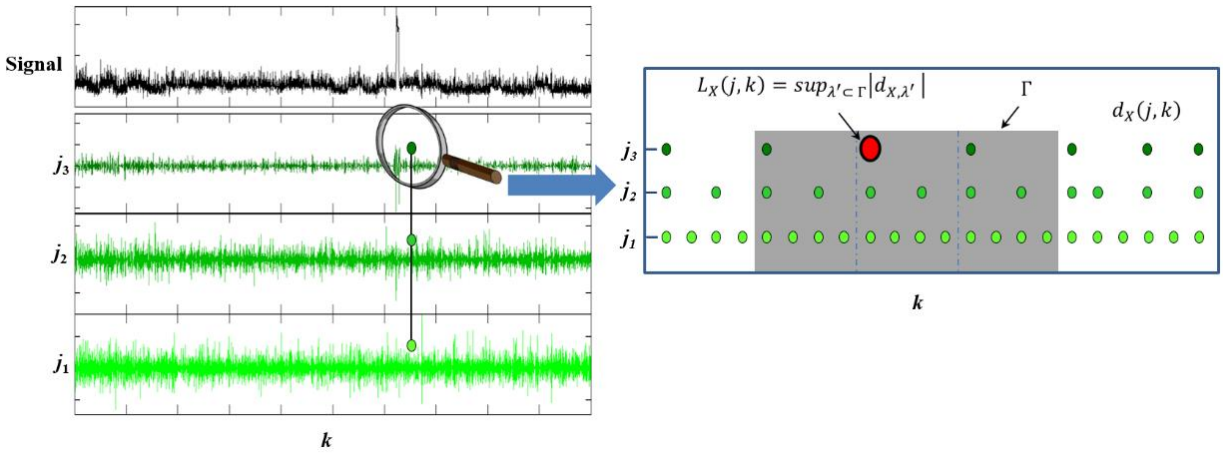

Fig. 4. Left: example of a voltage signal decomposition using the Daubechies wavelet 'db3'. Right: a zoom-in on the obtained wavelet coefficient details to give an illustration of the principle used in tracking the wavelet leaders L_X (black and red circle). They are calculated from the discrete wavelet coefficients $d_X(j,k)$ (green dots) by taking the supremum in the time neighborhood $\Gamma = 3\lambda$ over all finer scales $2^{j'} \leq 2^j$ (area in gray). (For interpretation of the references to color in this figure legend, the reader is referred to the web version of this article.)

The purpose of multifractal analysis (or singularity analysis) is to compute an analysis tool, namely a singularity spectrum (Fig. 3). This characterization is obtained by analyzing the behavior of structure functions, based on the WLMF approach, in the limit of small scales.
Let us define the structure functions $S_L(q,j)$, which quantify the spatial average of wavelet coefficients at a given scale 2^j:

$$S_L(q,j) = \frac{1}{n_j}\sum_{k=1}^{n_j}|L_X(j,k)|^q \quad (6)$$

Where q is the order of the statistical moment, $n_j \approx n / 2^j$ is the number of leaders available at each scale, and n the length of the sample [18].

The multifractal formalism consists in evaluating the behavior of the logarithm of structure functions in the limit of fine scales. This characterization [17] is given by the scaling exponents $\xi_L(q)$:

$$\xi_L(q) = \lim_{j\to 0} \inf \left(\frac{\log_2 S_L(q,j)}{j}\right) \quad (7)$$

In other terms, the structure functions $S_L(q,j)$ exhibit a power law behavior with respect to the scale analysis, in the limit of fine scales, and where C_q is a constant:

$$S_L(q,j) \cong C_q 2^{j\xi_L(q)} \quad (8)$$

The singularity spectrum representing the function $h \mapsto D(h)$ is obtained by the Legendre transform of the scaling exponents:

$$D_q(h) = \inf_{q\neq 0}(1 + qh - \xi_L(q)) \quad (9)$$

Let us consider the concept of the Hölder exponent. A positive exponent indicates that the function is continuous and has a given number of derivatives. A negative exponent implies that the function encloses transitions, jumps, and eventually divergences to infinity. As the last characteristics are not observed in the studied voltage signals, we must avoid all negative values of h and $D(h)$.
To obtain the $D(h)$ entire curve by the Legendre transform given by Eq. (9), both positive and negative values of q-order are needed: $q \in [q^-, q^+]$. Note that $q = q^-$ and $q = q^+$ amplify the small and large fluctuations of the signal.
In this study, both q^- and q^+ are selected to avoid the negative values of the Hölder exponent h and Hausdorff dimension $D(h)$. So, in the case of our study: $q = -4: 0.5: +5$ giving 19 values of h and 19 other values of $D(h)$.

4. Voltage Singularity Spectrum (VSS) as diagnosis tool

In this work, we propose to study the portability of the new diagnosis tool based on the investigation of singularity measurements stamped in FC stack voltage signals. Indeed, measuring local singularities on voltage signals provides suitable information about the evolving dynamics of non-stationary and non-linear processes involved in FC systems.
We assess the generalization and the usefulness of the proposed VSS by establishing the diagnosis on two databases issued from the two investigated PEMFC stacks.

For the stack $PEMFC_{Auto}$, 10 scenarios are analyzed (normal and abnormal conditions including one fault or more complex situations with 2 or 3 faults occurred simultaneously).
For the stack $PEMFC_{\mu CHP}$, 9 operating conditions (normal and abnormal conditions) are studied.

In this aim, we use 30 voltage profiles for each FC operating condition; each voltage profile covers 1000 voltage samples acquired at a frequency f_a =11Hz (Fig. 5) using the monitoring data system of the FC experimental test bench.

To perform the VSS, the analyzing wavelet is selected as Daubechies 3 ('Db3') function (with 3 vanishing moments, Fig. 5). Some examples of VSS computed for the normal conditions and abnormal ones are displayed in Fig. 6. As we can observe, the two VSS corresponding to DFSC (cathode flow fault) and DT (cooling circuit temperature fault) are shifted from the VSS linked with the normal conditions (Ref). Each operating condition set gives its own stamp in the morphology of the stack voltage signal, thus characterized by a VSS with specific shape, width, and location. The multifractal parameters can therefore be used as discriminant parameters for the diagnosis.
For the faulty operating conditions FSC = 1.3 or T = 72°C, the obtained VSS curves indicate clear differences in the values of the singularity features h_0, h_{min}, and h_{max} (these VSS features were described in Fig. 3). The features identification of the VSS plotted in Fig. 6 leads to:

$h_0 = 0.53, h_{min} = 0.28,$ and $h_{max} = 0.92$ for the normal operating conditions,
$h_0 = 0.46, h_{min} = 0.15,$ and $h_{max} = 0.95$ for DFSC,
$h_0 = 0.48, h_{min} = 0.19,$ and $h_{max} = 0.82$ for DT.

These results reveal a high multifractality and an irregularity degree of the voltage signal enhanced by the poor operating conditions resulting from the cathode flow fault and / or the cooling circuit temperature fault (overall, the two faulty VSS of Fig. 6 are shifted to the left from the normal conditions). This can be related with problems of air diffusion when the stack is supplied with a lower cathode flow rate (DFSC), and with a FC drying state when the stack temperature exceeds the nominal value (DT).

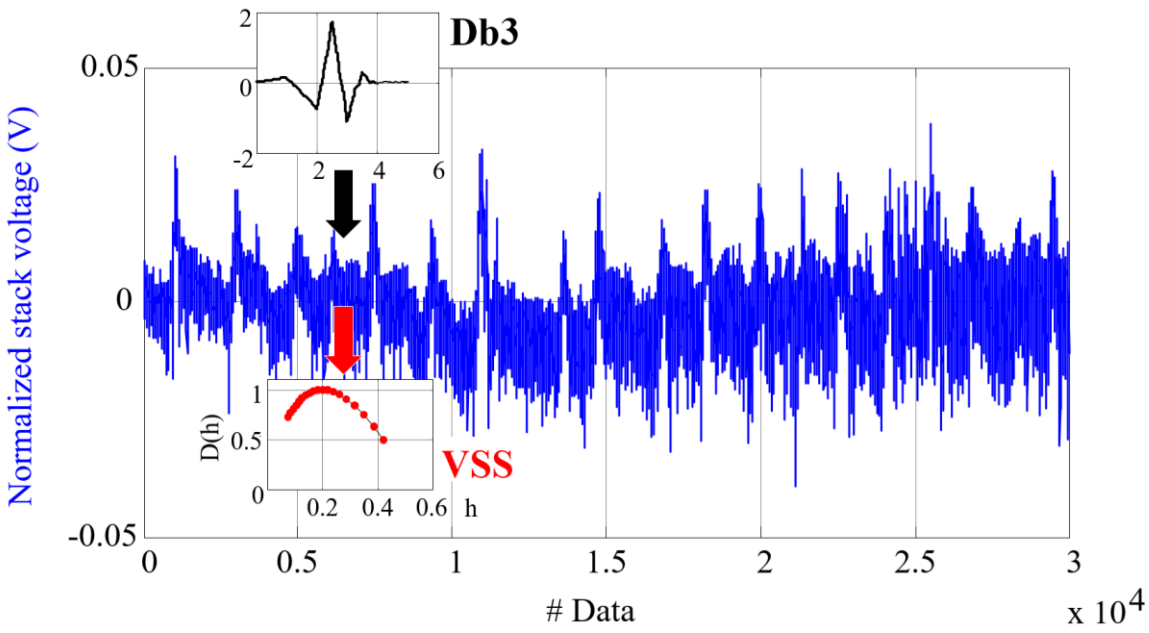

Fig. 5. Stack voltage signal scanned by Daubechies wavelet (Db3) for VSS computing.

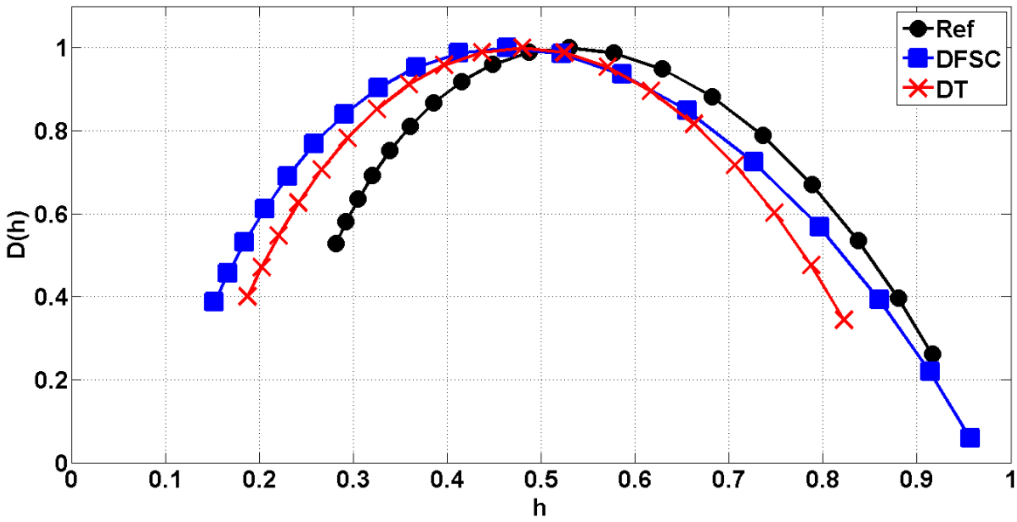

Fig. 6. Examples of VSS computed on profiles covering 1000 stack voltage samples; for the PEMFC nominal operating conditions (Ref) and for two examples of faults: a cathode flow fault (DFSC) and a cooling circuit temperature fault (DT).

Singularity features are then used to supply the Machine Learning approach, named K-Nearest Neighbors (KNN). KNN is a non-parametric learning algorithm, which consists in assigning unlabeled features to the class of the most similar labeled examples. The similarity can be estimated by using Euclidean metric for example.

To improve the performance of the fault classification method, the minimum Redundancy - Maximum Relevance (mRMR) technique [12,24] is used to select some relevance features offering the best classification rates. The mRMR feature selection technique was recently introduced for gene selection application [24].

This method is based on the mutual information estimates, which reveals the statistical dependence of a feature (x) on an another (y) [12].
$I(x,y)$ is the mutual information between x and y. It is computed as the relative entropy between the joint probabilistic distribution $p(x,y)$ and the product of marginal distributions probabilities $p(x)$ and $p(y)$:

$$I(x,y) = \sum_{x,y \in S} p(x,y) log\left(\frac{p(x,y)}{p(x).p(y)}\right) \quad (10)$$

Where S is the set of features.

The mRMR feature set is obtained by optimizing the following conditions *Redundancy Minimization* and *Relevance Maximization*:

- *Redundancy Minimization*:

$$\min Redundancy(x) = \frac{1}{|S|} \sum_{x,y \in S} I(x,y) \quad (11)$$

Where $|S|$ is the size of the set of features.

- *Relevance Maximization*:

$$\max Relevance(x) = \frac{1}{|S|} \sum_{x \in S} I(C,x) \quad (12)$$

Where $C = \{c1, c2 \dots cn\}$ is the set of the class labels.

The feature score is obtained by combining the two criteria expressed by Eq. (11) and (12):

$$Score(x) = \frac{Relevance(x)}{Redundancy(x)} \quad (13)$$

Or

$$Score(x) = Relevance(x) - Redundancy(x) \quad (14)$$

Equation (13) expresses the Mutual Information Difference (MID) criterion and Eq. (14) indicates the Mutual Information Quotient (MIQ) criterion.

Actually, 20 VSS / class are used to generate the learning database and the 10 others serve as test data to evaluate the performances of the classifier. Each VSS contains 38 features (19 h data and 19 $D(h)$ data). So, by applying the mRMR method on the full feature set (38 features) of the VSS combined with 8 statistical moments of the voltage, the good classification rate obtained using the top 6 selected features is about 89.4 % for the stack $PEMFC_{Auto}$, separating 10 classes (10 FC operating conditions). For the second stack $PEMFC_{\mu CHP}$, 9 classes are discriminated with a success of 95.5 %.

The best results of the classification rates of the different operating conditions studied are embedded in confusion matrixes given by Tables 4 and 5, for the stacks $PEMFC_{Auto}$ and $PEMFC_{\mu CHP}$ respectively.

Table 4. Confusion matrix of the good classification rates obtained with mRMR and kNN from the VSS computed with the stack voltage signals of the $PEMFC_{Auto}$. The studied FC operating conditions are: **Ref**: normal conditions - **DFSC**: cathode flow fault (slight air starvation) - **DFSA**: anode flow fault (slight H_2 starvation) - **DP**: gas pressure fault (lower gas pressure) - **DT**: cooling circuit temperature fault (lower stack temperature) - **DCO**: carbon monoxide poisoning (H_2+CO).

Class	C_0	C_1	C_2	C_3	C_4	C_5	C_6	C_7	C_8	C_9
Ref	**87.5**	0	0	12.5	0	0	0	0	0	0
DFSC	0	**100**	0	0	0	0	0	0	0	0
DFSA	0	0	**100**	0	0	0	0	0	0	0
DP	50	0	0	**50**	0	0	0	0	0	0
DT	0	0	0	0	**100**	0	0	0	0	0
DCO	0	0	0	0	0	**100**	0	0	0	0
DFSC & DP	0	0	0	0	0	0	**100**	0	0	0
DFSA & DP	0	0	0	0	0	0	0	**71.43**	28.57	0
DFSC & DFSA	0	0	0	0	0	0	0	0	**100**	0
DFSC & DFSA & DP	0	0	0	0	0	0	0	0	0	**100**

With: $C_0 \equiv \widehat{Ref}, C_1 \equiv \widehat{DFSC}, C_2 \equiv \widehat{DFSA}, C_3 \equiv \widehat{DP}, C_4 \equiv \widehat{DT}, C_5 \equiv \widehat{DCO}, C_6 \equiv \widehat{DFCS\ \&\ DP}$,
$C_7 \equiv \widehat{DFSA\ \&\ DP}, C_8 \equiv \widehat{DFSC\ \&\ DFSA}, C_9 \equiv DFSC\ \&\ \widehat{DFSA\ \&\ DP}$.

Table 5. Confusion matrix of the good classification rates obtained with mRMR and kNN from the VSS computed with the stack voltage signals of the $PEMFC_{\mu CHP}$. The studied FC operating conditions are: **Ref** : normal conditions - **DFSC**$^{\nearrow}$: cathode flow fault (air over-supply) - **DFSC**$_{\searrow}$: cathode flow fault (slight air starvation) - **DFSA**$^{\nearrow}$: anode flow fault (H_2 over-supply) - **DFSA**$_{\searrow}$: anode flow fault (H_2 starvation) - **DT**$^{\nearrow}$: cooling circuit temperature fault (higher temperature) - **DT**$_{\searrow}$: cooling circuit temperature fault (lower stack temperature) - **DRH**$^{\nearrow}$: gas dew point temperature fault (higher dew point temperatures) - **DRH**$_{\searrow}$: gas dew point temperature fault (lower dew point temperatures).

Class	C_0	C_1	C_2	C_3	C_4	C_5	C_6	C_7	C_8
Ref	**100**	0	0	0	0	0	0	0	0
DFSC↗	0	**100**	0	0	0	0	0	0	0
DFSC↘	0	0	**100**	0	0	0	0	0	0
DFSA↗	0	0	0	**90**	0	10	0	0	0
DFSA↘	0	0	0	0	**90**	0	0	0	10
DT↗	0	0	0	20	0	**80**	0	0	0
DT↘	0	0	0	0	0	0	**100**	0	0
DRH↗	0	0	0	0	0	0	0	**100**	0
DRH↘	0	0	0	0	0	0	0	0	**100**

With: $\boldsymbol{C_0} \equiv \widehat{Ref}$, $\boldsymbol{C_1} \equiv \widehat{DFSC}^{\nearrow}$, $\boldsymbol{C_2} \equiv \widehat{DFSC}_{\searrow}$, $\boldsymbol{C_3} \equiv \widehat{DFSA}^{\nearrow}$, $\boldsymbol{C_4} \equiv \widehat{DFSA}_{\searrow}$, $\boldsymbol{C_5} \equiv \widehat{DT}^{\nearrow}$, $\boldsymbol{C_6} \equiv \widehat{DT}_{\searrow}$,
$\boldsymbol{C_7} \equiv \widehat{DRH}^{\nearrow}$, $\boldsymbol{C_8} \equiv \widehat{DRH}_{\searrow}$.

Overall, as we can see in Tables 4 and 5, the proposed diagnosis strategy identifies successfully several complex operating faults (i.e. slight deflections from the nominal operating conditions, and even combination of faults) for both $PEMFC_{Auto}$ and $PEMFC_{\mu CHP}$. The diagnosis strategy, though, has difficulty separating the pressure fault condition (DP) from the nominal one (Table 4). The fault related with the pressure parameter, introduced with the level P=1.3 bar abs and

corresponding to a small deviation from the nominal value (P=1.5 bar abs), had very little effect on the PEMFC operation and thus did not really alter the morphology of the stack voltage signal.

Recent works reported in the literature are dealing with the FC diagnosis issue. We have selected two examples of interesting papers, which are closely related with our approach. It is not easy to compare directly the results obtained using the different approaches, especially since the databases and the fault considered differ more or less. However, some main points of comparison can be given below.
In their paper [25], Zheng et al. present a novel method for PEMFC diagnosis based on artificial neural networks, named Reservoir Computing 'RC', also based on the measurement of the stack voltage signal. In this work, five simple faults are studied, namely: CO poisoning, low air flowrate, defective cooling, and natural degradation. The studied data are similar to ours. However, FC operating scenarios combining two or three faults are not considered. Zheng et al. mention in their article that the fault recognition rate (classification rate) is influenced by four key RC parameters and by the order in the learning database. However, even in the worst case, the good classification rate reaches 88%.
In the work of Li et al. [16], the PEMFC individual cell voltages are selected as the variables leading to the FC diagnosis. Five operating conditions are considered: nominal conditions, low pressure level, high pressure level, high cathode stoichiometry, and low relative humidity. The diagnosis strategy was implemented on-line successfully. The fault detection task is performed by applying Support Vector Machine (SVM) as the pattern classification tool. In our approach, the diagnosis tool is based on the only free evolution of the stack voltage, with reduces the required instrumentation. In addition, more complex fault situations, including combinations of faults, are considered in our work.

5. Conclusions

In this study, VSS are computed on voltage signals acquired under different FC operating conditions (normal and abnormal, i.e. more or less severe deviations from the normal conditions) with considering situations that combine 2 or 3 faults simultaneously. Two stacks are investigated: a $PEMFC_{Auto}$ stack that is designed for automotive applications and a $PEMFC_{\mu CHP}$ stack, dedicated to stationary ones.
Singularity features extracted from the estimated VSS are classified using Machine Learning approach, named K-Nearest Neighbors (KNN).
The obtained classification results show that the proposed PEMFC diagnosis tool allows identifying simple operating faults and more complicated states that contain several fault types. The diagnosis are realized on two different test stands, for different stack sizes, powers and technologies, with different targeted environments of power application.
In this paper, we demonstrate that the singularity analysis of voltage signal offers a generic diagnosis tool for the PEMFC SoH monitoring. One key-point of the method is that the VSS can be estimated from the "free" evolution of the stack voltage and without affecting the FC operation in any way: no external additional solicitation is required to reveal the SoH patterns.

Acknowledgement
The work performed was done thanks to the French ANR project "DIAPASON 2" (ANR-10-HPAC-0002)) and in the framework of the "Decentralized energy production" project, directed by EFFICACITY, the French R&D Institute for urban energy transition.

References

[1] Fuel Cell Industry Review 2015: http://www.fuelcellindustryreview.com.

[2] M Buchholz, V Brebs. Dynamic Modelling of a Polymer Electrolyte Membrane Fuel Cell Stack by Nonlinear System Identification. Fuel Cells 2007; 7:392-401.

[3] J Mainka, G Maranzana, A Thoaq, J Dillet, S Didierjean, O Lottin. One-dimensional Model of Oxygen Transport Impedance Accounting for Convection Perpendicular to the Electrode. Fuel Cells 2012; 12(5):848-861.

[4] S Chevalier, B Auvity, JC Olivier, C Josset, D Trichet, M Machmoum. Multiphysics DC and AC models of a PEMFC for the detection of degraded cell parameters. International Journal of Hydrogen Energy 2013; 38(26):11609-11618.

[5] R Petrone, Z Zheng, D Hissel, MC Péra, C Pianese, M Sorrentino, M Béchérif, N Yousfi Steiner. A review on model-based diagnosis methodologies for PEMFCs. International Journal of Hydrogen Energy 2013; 38:7077-7091.

[6] Z Zheng, R Petrone, MC Péra, D Hissel, M Béchérif, C Pianese, N Yousfi Steiner, M Sorrentino. A review on non-model based diagnosis methodologies for PEM fuel cell stacks and systems. International Journal of Hydrogen Energy 2013; 38(21):8914-8926.

[7] S Giurgia, S Tirnovan, D Hissel, R Outbib. An analysis of fluidic voltage statistical correlation for a diagnosis of PEM fuel cell flooding. International Journal of Hydrogen Energy 2013; 38(11):4689-4696.

[8] Z Li, R Outbib, D Hissel, S Giurgia. Data-driven diagnosis of PEM fuel cell: A comparative study. Control Engineering Practice 2014; 28:1-12.

[9] J Chen, B Zhou. Diagnosis of PEM fuel cell stack dynamic behaviors. Journal of Power Sources 2008; 177:83-95.

[10] MA Rubio, K Bethune, A Urquia, J St-Pierre. Proton exchange membrane fuel cell failure mode early diagnosis with wavelet analysis of electrochemical noise. International Journal of Hydrogen Energy 2016; 41:14991-15001.

[11] N Yousfi Steiner, D Hissel, P Moçotéguy, D Candusso. Non intrusive diagnosis of polymer electrolyte fuel cells by wavelet packet transform. International Journal of Hydrogen Energy 2011; 36:740-746.

[12] D Benouioua, D Candusso, F Harel, L Oukhellou. PEMFC stack voltage singularity measurement and fault classification. International Journal of Hydrogen Energy 2014; 39(36):21631-21637.

[13] D Benouioua, D Candusso, F Harel, L Oukhellou. The dynamic multifractality in PEMFC stack voltage signal as a tool for the aging monitoring. International Journal of Hydrogen Energy 2017; 42(2):1466-1471.

[14] D Hissel, D Candusso, F Harel. Fuzzy-Clustering durability diagnosis of Polymer Electrolyte Fuel Cells dedicated to transportation applications. IEEE Transactions on Vehicular Technology 2007; 56(5):2414-2420.

[15] J Kim, I Lee, Y Tak, BH Cho. State-of-Health diagnosis based on hamming neural network using output voltage pattern recognition for a PEM fuel cell. International Journal of Hydrogen Energy 2012; 37(5):4280-4289.

[16] Z Li, R Outbib, S Giurgia, D Hissel, S Jemeï, A Giraud, S Rosini. Online implementation of SVM based fault diagnosis strategy for PEMFC systems. Applied Energy 2016; 164:284-293.

[17] S Jaffard, B Lashermes, P Abry. Wavelet leaders in multifractal analysis, in Wavelet Analysis and Applications. Ed. Birkhäuser Verlag. 2006.

[18] H Wendt, P Abry. Multifractality Tests Using Bootstrapped Wavelet Leaders. IEEE Transactions on Signal Processing 2007; 55(10):4811-4820.

[19] D Benouioua, D Candusso, F Harel, L Oukhellou. Multifractal analysis of stack voltage based on wavelet leaders: A new tool for PEMFC diagnosis. Fuel Cells 2017; 17(2):217-224.
[20] BB Mandelbrot. Fractals Geometry of Nature. Edition. Freeman, San Francisco. 1982.
[21] P Balança. Some sample path properties of multifractional Brownian motion. Stochastic Processes and their Applications 2015; 125(10):3823-3850.
[22] L Chevillard, B Castaing, E Lévêque, A Arneodo. Unified multifractal description of velocity increments statistics in turbulence: Intermittency and skewness. Physica D 2006; 218:77-82.
[23] D Grech. Alternative measure of multifractal content and its application in finance. Chaos, Solitons and Fractals 2016; 88:183-195.
[24] Hanchuan Peng's web site. Information on mRMR (minimum Redundancy Maximum Relevance Feature Selection). http://home.penglab.com/proj/mRMR/. 2017.
[25] Z Zheng, S Morando, M-C Péra, D Hissel, L Larger, R Martinenghi, AB Fuentes. Brain-inspired computational paradigm dedicated to fault diagnosis of PEM fuel cell stack. International Journal of Hydrogen Energy 2017; 42(8):5410-5425.

Figure captions:

Fig. 1. Pictures of the two investigated PEMFC stacks:
a) 8 cell stack designed for automotives ($PEMFC_{Auto}$),
b) 12 cell stack designed for µCHP operation ($PEMFC_{\mu CHP}$).

Fig. 2. Illustration of two pointwise regularity measures in the signal $X(t)$ quantified by the Hölder exponent h.

Fig. 3. Example of a singularity spectrum $D(h)$.

Fig. 4. Left: example of a voltage signal decomposition using the Daubechies wavelet 'db3'. Right: a zoom-in on the obtained wavelet coefficient details to give an illustration of the principle used in tracking the wavelet leaders L_X (red circle). These last ones are calculated from the discrete wavelet coefficients $d_X(j,k)$ (green dots) by taking the supremum in the time neighborhood $\Gamma = 3\lambda$ over all finer scales $2^{j'} \leq 2^j$ (area in gray).

Fig. 5. Stack voltage signal scanned by Daubechies wavelet (Db3) for VSS computing.

Fig. 6. Examples of VSS computed on profiles covering 1000 stack voltage samples; for the PEMFC nominal operating conditions (Ref) and for two examples of faults: a cathode flow fault (DFSC) and a cooling circuit temperature fault (DT).

Table captions:

Table 1. $PEMFC_{Auto}$ nominal operating conditions.

Table 2. $PEMFC_{\mu CHP}$ nominal operating conditions.

Table 3. The set of FC operating conditions applied during the experimentation of the two stacks: **Ref**: normal conditions - **DFSC**: cathode flow fault - **DFSA**: anode flow fault - **DP**: gas pressure fault - **DT**: cooling circuit temperature fault - **DRH**: gas dew point temperature fault - **DCO**: carbon monoxide poisoning (H_2+CO).
The underlying parameter values correspond to the introduced faults.
The notation 'ND' means that the experiment is Not Done.

Table 4. Confusion matrix of the good classification rates obtained with MRMR and kNN from the VSS computed with the stack voltage signals of the $PEMFC_{Auto}$. The studied FC operating conditions are: **Ref**: normal conditions - **DFSC**: cathode flow fault (slight air starvation) - **DFSA**: anode flow fault (slight H_2 starvation) - **DP**: gas pressure fault (lower gas pressure) - **DT**: cooling circuit temperature fault (lower stack temperature) - **DCO**: carbon monoxide poisoning (H_2+CO).

Table 5. Confusion matrix of the good classification rates obtained with mRMR and kNN from the VSS computed with the stack voltage signals of the $PEMFC_{\mu CHP}$. The studied FC operating conditions are: **Ref** : normal conditions - $\mathbf{DFSC}^{\nearrow}$: cathode flow fault (air over-supply) - $\mathbf{DFSC}_{\searrow}$: cathode flow fault (slight air starvation) - $\mathbf{DFSA}^{\nearrow}$: anode flow fault (H_2 over-supply) - $\mathbf{DFSA}_{\searrow}$: anode flow fault (H_2 starvation) - $\mathbf{DT}^{\nearrow}$: cooling circuit temperature fault (higher temperature) - $\mathbf{DT}_{\searrow}$: cooling circuit temperature fault (lower stack temperature) - $\mathbf{DRH}^{\nearrow}$: gas dew point temperature fault (higher dew point temperatures) - $\mathbf{DRH}_{\searrow}$: gas dew point temperature fault (lower dew point temperatures).